General Interface for Power Management of Micro-Grids Using Nonlinear Cooperative Droop Control

Seyed Mahdi Ashabani and Yasser Abdel-Rady I. Mohamed, *Senior Member, IEEE*

***Abstract*—This paper presents a comprehensive and general nonlinear control/power management strategy for both converter- and synchronous-machine-based units in microgrids. The proposed controller offers the following advantages as compared to previously reported controllers: 1) It can fulfill requirements of both islanded and grid connected microgrids without a need for reconfiguration; 2) the controller-manager adopts cascaded angle, frequency and power control loops, which give enhanced power sharing accuracy and nominal-frequency operation at steady-state conditions (i.e., permanent frequency drop is eliminated); 3) the controller provides an emulated performance of synchronous machines with controllable damping and synchronization power components, which provide additional degrees of freedom to improve the dynamic performance of the system and easy integration in systems with multiple converters synchronous machines; 4) the controller is equipped with a nonlinear supplementary controller to mitigate large power angle swings associated with large-signal disturbances; 5) the controller can be easily adapted to conventional synchronous machines; and 6) the controller provides seamless operation under out-of-phase reclosing. The proposed controller can realize the concept of plug-and-play of DG units and micrgrids in smart power environment. The effectiveness of the controller to damp power oscillations and ensure system seamless performance in a wide range of operating conditions is validated by simulation results under various microgrid operating scenarios.**

***Index Terms*—Droop control, microgrids, power converters, power management, stability, synchronous machines.**

NOMENCLATURE

P	DG output active power.
Q	DG output reactive power.
P^*_{SG}	Power set-point of synchronous generator's droop characteristic.
P^*	Power set-point of VSC's droop characteristic.
E	VSC voltage amplitude.
V_L	Local load bus voltage amplitude.
δ	VSC voltage angle.
δ_L	Local load bus voltage angle.
δ_{DG}	Load angle $(\delta - \delta_L)$.
δ_{set}	Set angle in drooping control.
R_F	Filter resistance.
X_F	Filter reactance.
R_T	Transformer resistance.
X_T	Transformer reactance.
Z_T	Transformer impedance.
R	Total connecting resistance.
X	Total connecting reactance.
R_L	Line resistance.
X_L	Line reactance.
ω	VSC frequency.
ω_{rotor}	Synchronous generator's rotor speed.
ω_L	Local load bus frequency.
ω_{set}	Set frequency (rated frequency).
ω_0	Set frequency of drooping control.
E_0	Set voltage of drooping control.
m	Frequency versus real power slope constant.
n	Voltage versus reactive power slope constant.
d	Angle versus real power slope constant.
K_f	Power-frequency characteristics slope.
K_d	Power-angle characteristics slope.
K_p	Power loop integrator gain.
k_i	Nonlinear control law gains, $k_i > 0$.
J	Rotor momentum of inertia.
$\Delta\omega_{\max}$	Maximum acceptable frequency drop.
$\Delta E_{\max}$	Maximum acceptable voltage drop.
P_{damp}	Damping power.
P_{synch}	Synchronizing power.
θ	System augmented uncertainty.
$\widehat{\theta}$	Estimation of system uncertainty.

Manuscript received July 07, 2012; revised November 27, 2012 and March 05, 2013; accepted March 08, 2013. Date of publication April 25, 2013; date of current version July 18, 2013. Paper no. TPWRS-00689-2012.

The authors are with the Department of Electrical and Computer Engineering, University of Alberta, Edmonton, AB T6G2V4, Canada (e-mail: ashabani@ualberta.ca; yasser_rady@ieee.org).

Color versions of one or more of the figures in this paper are available online at http://ieeexplore.ieee.org.

Digital Object Identifier 10.1109/TPWRS.2013.2254729

γ	Adaptation law gain.
u	Control input.
u_f	Mapped control input.
P_{prim}	Primary source reference power command.
P_m	Input mechanical power of synchronous generator.
P_{out}	Output real power of synchronous generator.
P_{set}	Set real power of VSC.
τ_p	Primary source time constant.

I. Introduction

THE development of the distributed generation (DG) concept has changed the paradigm of energy generation and transfer under the smart grid vision [1]. DG units can be empowered by clean or renewable resources, such as fuel cells, photovoltaic (PV), micro-turbines and wind turbines. Due to fast development of power electronic devices, the majority of DG units are interfaced to the grid through power converters. A cluster of DG units, loads and energy storage systems connected together form a microgrid (MG) which can operate in three modes of operation, namely 1) grid connected mode, 2) islanded mode and 3) transition between the two modes [2], [3]. The concept of MG has been expanded to overcome the common interconnection issues contributed from individual DG units [4]–[6]. With appropriate integration and control of MGs, better reliability, power quality, customer satisfaction, voltage profile and increased efficiency due to loss minimization can be yielded. The MG concept provides a new level of controllability in smart grid paradigm [7]. However, since DGs and MGs are widely distributed over the network, their observability and controllability are key issues in distribution system operation and control [8], [9].

The main issues of MG operation are interactions between DG units and the main grid, frequency control and regulation in islanded mode [1], [8], [10], accurate power sharing in islanded mode to avoid circulating current among DG units, seamless transition between grid-connected and islanded modes, and robust stable operation during contingencies, such as sudden large power variations, out-of-phase reclosing and fault conditions. The stability issues related to MG operation are mainly contributed to the lack of dominant energy resources in autonomous mode, different response time constants of electronically coupled (EC) DG and conventional generators, lack of inertia for frequency dynamics in EC-DG units, which may lead to angle/voltage instability [3], and instabilities due to change of mode of operation. The main control strategies proposed for microgrids are [11], the centralized approach [12]–[14], the master-slave technique [15] and frequency/angle and voltage droop [6], [16]–[18]. Among them, since droop control utilizes only local information, it is the most adopted control technique for MGs to enhance system reliability and realize a complete autonomous control structure. The main objective of the droop control during islanding mode is to share total MG real and reactive powers demand among DG units according to their power capacities [10], [16]. In grid connected mode, DG units are required to generate preset real and reactive powers (P-Q bus) or generate preset real power at constant bus voltage (P-V bus). In spite of their advantages, the conventional droop controllers have several drawbacks. Important among these are poor frequency regulation due to variable frequency operation, poor power sharing because of unmatched line impedances, low stability margin [10], [19], lack of ability to work in all operational modes without reconfiguration, and transients associated with transitions between grid connected and islanding modes. It is well known that better power sharing accuracy can be achieved at the cost of lower stability margin. That is to say, there is a tradeoff between frequency regulation, system stability and accurate power sharing. Stability of a droop-controlled MG can be improved using either supplementary control [20] or adaptive droop gains [10], [21]. To mitigate problems associated with the conventional droop control, an alternative approach is to use load angle droop instead of frequency droop [20], [22], [23]. The angle droop provides a constant frequency operation which is the main benefit; however, it suffers from poor power sharing and low stability margin. This is more pronounced when the load angle is large [22].

This paper proposes a general control strategy, for both converter- and synchronous-machine-based DG units in MGs, based on a combined angle-frequency droop controller with improved dynamic performance. As compared to previous autonomous control strategies [1]–[23], the proposed controller has the following advantages. 1) The proposed strategy combines frequency and angle droop strategies, therefore better power sharing accuracy can be obtained. In addition, designer has more degrees of freedom to select droop gains since there are two droop loops. Satisfactory static and dynamic performances can be simultaneously fulfilled by proper selection of these two constants. 2) It has a general structure for grid-connected and isolated modes of operation without a need for reconfiguration. This helps to mitigate problems due to islanding detection delay or non-detection zones and controller strategy changes subsequent to islanding. 3) The MG presents better power quality with steady-state nominal frequency operation which is an essential feature for many applications. 4) A nonlinear controller is designed to assist the angle-frequency droop controller. It provides a supplementary additional signal for the voltage control loop. The duty of the nonlinear controller is to preserve large-signal stability of the MG when severe contingencies, such as transition to islanding, out-of-phase closing and DG reconnection occur. Linear controllers which are designed to account for small variations around a specific operating point may fail during these situations, thus a nonlinear controller which guarantees system stability even during large variations of operating point is of high interest. 5) Virtual inertia function is embedded within the control loops; therefore, the frequency and voltage dynamics of DG units become similar to the corresponding dynamics of conventional synchronous generators (SGs) [24]. With this approach, converter-based units (e.g., voltage-source converters (VSCs) mimic the dynamic behavior of SGs. In other words, the controller presents inertia and damping dynamics for frequency and angle similar to an SG. This virtual inertia can significantly improve power system dynamic performance and frequency regulation especially in converter-dominated

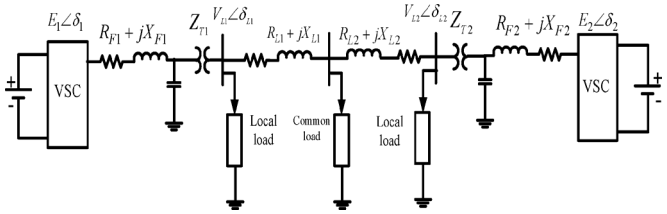

Fig. 1. Two-DG microgrid.

grids where grid equivalent rotational inertia is low [25]–[27]. This helps to overcome problems due to fast response of VSCs and interactions between SGs and VSCs [3], [28]. Furthermore, the frequency inertia mitigates the frequency chattering phenomenon caused by rapid load power changing in an MG. Time-domain simulation results are presented to demonstrate the effectiveness of the proposed controller to damp power oscillations and ensure MG seamless performance in a wide range of operating conditions.

II. Theory of Power Sharing

Without loss of generality, the theory of power sharing is explained using a two-DG MG as shown in Fig. 1. Each DG is connected to its local load bus through connecting impedance $(R + jX)$ including filter $(R_F + jX_F)$ and transformer impedances $(R_T + jX_T)$, the load bus is connected to the PCC thorough line impedance $(R_L + jX_L)$. The real and reactive powers of each DG unit supplied to the bus are given by

$$P = \frac{E}{R^2 + X^2}(XV_L \sin\delta_{\rm DG} + R(E - V_L \cos\delta_{\rm DG})) \quad (1)$$

$$Q = \frac{E}{R^2 + X^2}(RV_L \sin\delta_{\rm DG} + X(E - V_L \cos\delta_{\rm DG})). \quad (2)$$

The connecting impedance (X and R) between each DG and the load bus consists of filter and transformer impedances, which indicates that P and Q are highly coupled in resistive lines. In highly inductive lines, the injected real power is mainly regulated by the load angle $\delta_{\rm DG}$ whereas reactive power is regulated by VSC voltage amplitude (E).

In the conventional droop control, the frequency (ω) and voltage amplitude are obtained as

$$\omega = \omega_0 - mP \quad (3)$$

$$E = E_0 - nQ. \quad (4)$$

The frequency and voltage droops form a communication-free medium to share real and reactive power among DG units proportional to their power capacities. In fact, frequency and voltage set-points are used as global virtual communication signals between DG units. The droop constants are obtained based on this criterion and are given by

$$m = \frac{\Delta\omega_{\max}}{P_{\max}} \quad (5)$$

$$n = \frac{\Delta E_{\max}}{Q_{\max}}. \quad (6)$$

It is well understood that if droop coefficients are increased in autonomous mode, power sharing accuracy is improved at the cost of poor frequency and voltage regulation [21], [22]. It is also well known that higher droop gains adversely affect system stability and there are some limits to ensure system good performance and stability indicating some inherent tradeoff between power sharing accuracy, power quality, transient response, and system stability. An alternative for real power sharing is angle drooping. Unlike SGs, the output power angle of a VSC can be changed instantaneously without changing frequency; therefore using the angle droop is another way to share real power. As a matter of fact, since real power is controllable through load angle, there is no need to vary frequency to regulate power; thus, frequency is just employed as a medium for angle tuning. The governing equation in this case is as follows:

$$\delta = \delta_{\rm set} - dP. \quad (7)$$

The angle droop provides a constant frequency operation which is the main benefit; however, it suffers from poor power sharing and low stability margin which is more obvious when the load angle is large. To achieve accurate load sharing, a centralized control strategy using communication infrastructure was developed in [22] to adjust the load angle preset values online. However, it is not of high interest to embed communication infrastructure in decentralized droop control where its main goal is MG power management based on local information without data exchange with a centralized controller. Moreover, by increasing the angle droop gain or output power, a DG unit may be easily destabilized [10], [23].

III. Proposed Controller Topology

To overcome the aforementioned problems, a comprehensive control topology is presented in this paper. All control and power management requirements of an MG are augmented in one general control scheme. It involves angle, frequency and power loops and consequently benefit from their advantages simultaneously. Constant frequency operation and accurate power sharing can be realized by combined angle-frequency droop while large-signal stability of the system is achieved by a supplementary nonlinear controller.

Fig. 2 represents the block diagram of the overall power manager-controller proposed for a VSC-based DG unit. The controller is implemented in polar coordinates and directly regulates the output voltage vector amplitude and angle. As shown in Fig. 2, the frequency control loop has two cascaded angle and frequency loops which determine the reference power; and a power synchronization loop which adjusts the VSC output frequency based on the reference and actual active powers. This power synchronizing loop introduces virtual inertia for frequency as it mimics rotor momentum of inertia of a conventional SG [24]. The angle and frequency loops play two various roles; first, they behave like dampers to mitigate angle and frequency oscillations. Second, they provide synchronizing power. The damping and synchronizing power components [29] are given by

$$\text{Damping power} = \Delta P_{\rm damp} = -K_f \Delta\omega \quad (8)$$

$$\text{Synchronizing power} = \Delta P_{\rm synch} = -K_f K_d \Delta\delta. \quad (9)$$

The synchronizing power attempts to return load angle to its equilibrium point subsequent to transients while damping

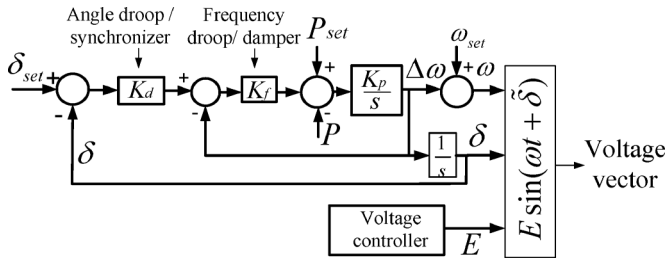

Fig. 2. Hybrid angle-frequency droop control.

power is responsible for preserving frequency stability and mitigating frequency oscillations. Hence, the proposed topology offers more damped transient behavior as compared to the conventional frequency or angle-droop controllers because of these extra loops. In autonomous mode, K_d and K_f act as angle and frequency droops while the angle droop is the main power sharing loop.

The frequency dynamics is similar to an SG, in which the rotating shaft is resisted by a viscous damping proportional to the frequency deviation and used as damping power. In the proposed topology, an extra damping (K_d) exists, which is responsible to damp angle oscillations, therefore, the controller offers better angle stability. The augmented dynamic equation is given by

$$\frac{d\Delta\omega}{dt} = -K_pK_f(\omega-\omega_{\rm set}) - K_dK_pK_f(\delta-\delta_{\rm set}) - K_p(P-P_{\rm set}), \quad (10)$$

The relationship between the VSC frequency and the load angle is

$$\frac{d\delta}{dt} = \Delta\omega. \quad (11)$$

As mentioned, in autonomous mode, two cascaded droop loops exist which cooperate with each other to share active power and also damp angle and frequency oscillations. The first angle droop loop generates the frequency reference for the second frequency droop loop according to the angle error

$$\Delta\omega_{\rm set} = K_d(\delta_{\rm set}-\delta). \quad (12)$$

Based on this frequency set-point, the frequency droop determines the power reference

$$\Delta P_{\rm set} = K_f(\Delta\omega_{\rm set}-\Delta\omega). \quad (13)$$

In stable steady-state conditions, the input to the integrator is zero. Thus

$$P = P^* - K_fK_d\delta - K_f\Delta\omega \quad (14)$$

where $P^* = P_{\rm set} + K_fK_d\delta_{\rm set}$. The angle and frequency droop gains are equal to $K_d \times K_f$ and K_f, respectively. From (14) it is concluded that K_f is proportional to the inverse of frequency droop (m) and $K_d \times K_f$ is equal to the inverse of angle droop (d).

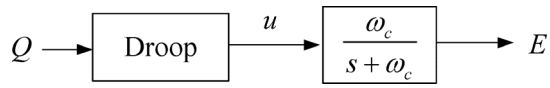

Fig. 3. Voltage controller.

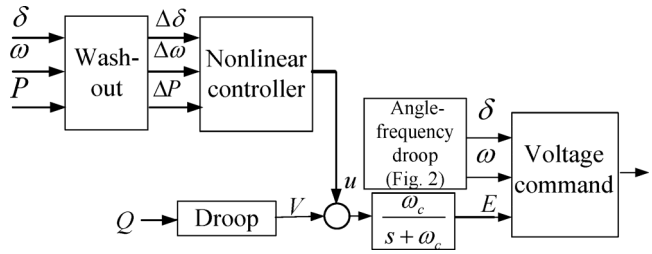

Fig. 4. Nonlinear supplementary controller.

The adopted topology for voltage amplitude control is shown in Fig. 3. It involves a voltage versus reactive power droop and a low-pass filter. The voltage droop is a tool to share the MG reactive power among DG units proportional to their power capacities. The voltage amplitude is obtained by processing the drooped voltage command by a low-pass filter. Actually, the existence of the low-pass filter presents additional dynamics for the voltage and resembles the flux decay behavior of an SG. As it will be shown in the next section, this voltage dynamics is useful during nonlinear controller design. It is worth noticing that the low-pass filter helps to eliminate high-order harmonics generated due to VSC switching behavior.

IV. Nonlinear Supplementary Controller Design

To design the supplementary nonlinear controller, the state-space model of the system is required. The supplementary nonlinear controller is illustrated in Fig. 4. As shown, this controller generates an additional signal for the linear controller of the voltage loop. The concept of supplementary voltage control has been originally derived from the power system stabilizer [29] in which an additional signal is added to the rotor excitation reference voltage to improve angle stability under system disturbances. In its conventional version, the power system stabilizer adopts power deviations as its input and it is processed by a lead-lag compensator to obtain the supplementary voltage-reference [29]. By proper tuning of the lead-lag controllers at a given operating point, angle stability can be enhanced; however, since the relation between the load angle and power is nonlinear, the linear controller may fall-short to ensure system stability in all operating points, particularly under large-signal transients. Similarly, according to (1), the load-angle equation is highly nonlinear and in an MG system, the nonlinearity is more pronounced because there is no base power. Therefore, DG output power and load angle may vary in a wide range. In this paper, the concept of power system stabilizer is adopted for VSCs where a nonlinear controller is designed to assure large-signal stability of each DG unit. The load angle, frequency and power are selected as state-space variables and the DG state-space model is given by

$$\dot{x}_1 = x_2 \quad (15)$$

$$\dot{x}_2 = a_1 x_1 + a_2 x_2 + a_3 x_3 \tag{16}$$

$$\dot{x}_3 = u_f + E\frac{V_L}{X} x_2 \cos x_1 - \omega_c x_3 + \theta \tag{17}$$

where u_f is related to the control input u by

$$u_f = u\omega_c \frac{V_L}{X} \sin x_1 \tag{18}$$

and

$$a_1 = -K_p K_f K_d, a_2 = -K_f K_p, a_3 = -K_p,$$
$$[x_1, x_2, x_3] = [\Delta\delta, \Delta\omega, \Delta P].$$

The term θ is added to (17) to account for system uncertainties including local and inter-area ones. This augmented disturbance rejection yields a more robust system and is estimated during nonlinear controller design using adaptive estimation technique. The adaptive backstepping technique is employed to design the nonlinear controller and overcome system uncertainties. The control design procedure is based on the following steps.

Firstly, the frequency reference $(x_{2\text{ref}})$ is calculated to stabilize the load angle δ. The Lyapunov function is selected as

$$V_1 = \frac{1}{2} x_1^2. \tag{19}$$

To stabilize x_1, $\dot{V}_1$ should be negative definite. Now, if

$$x_{2\text{ref}} = -k_1 x_1 \quad k_1 > 0 \tag{20}$$

then

$$\dot{V}_1 = -k_1 x_1^2 + x_1 e_2 \tag{21}$$

where $e_2 = x_2 - x_{2\text{ref}}$. According to (21), there is no guarantee that $\dot{V}_1 < 0$. In the next steps, by proper selection of $x_{3\text{ref}}$, $\dot{V}_1$ is made negative definite [30], [31].

To stabilize the frequency dynamics, $x_{3\text{ref}}$ is chosen according to the Lyapunov function

$$V_2 = V_1 + \frac{1}{2} e_2^2. \tag{22}$$

The derivative of V_2 along its trajectory is

$$\dot{V}_2 = \dot{V}_1 + e_2 \dot{e}_2 \tag{23}$$

where $\dot{e}_2 = \dot{x}_2 - \dot{x}_{2\text{ref}}$. Using (16) and (20), it follows that

$$\dot{e}_2 = \left[k_1 k_p k_f - k_p k_d k_f - k_1^2\right] x_1 + (k_1 - k_p k_f) e_2 + a_3 (e_3 + x_{3\text{ref}}). \tag{24}$$

If

$$x_{3\text{ref}} = c_1 x_1 + c_2 e_2 \tag{25}$$

where

$$c_1 = \frac{(1 - k_1(-a_2 + k_1) + a_1)}{a_3} \tag{26}$$

$$c_2 = -\frac{(k_1 + k_2 + a_2)}{a_3}, \quad k_2 > 0 \tag{27}$$

then $\dot{V}_2$ becomes

$$\dot{V}_2 = -k_1 e_1^2 - k_2 e_2^2 + a_3 e_2 e_3. \tag{28}$$

From (28), it is concluded that system (15)–(17) still is not fully stabilized and hence u_f should be designed in the next step to make $\dot{V}_2$ negative definite.

Finally, to obtain control input u_f, the Lyapunov function is defined as

$$V_3 = V_2 + \frac{1}{2} e_3^2 + \frac{1}{2}\gamma(\theta - \widehat{\theta})^2 \tag{29}$$

where θ and $\widehat{\theta}$ are the lump-sum uncertainty and its estimated value, respectively, and γ is the adaptation law gain. To ensure that $\dot{V}_2 < 0$, the Lyapunov function V_3 involves V_2, global stability of frequency is not confirmed, so in this step u_f is obtained in such a way that it guarantees stability of the Lyapunov functions V_2 and V_3 simultaneously. Now, consider the dynamics of

$$\dot{e}_3 = \dot{x}_3 - \dot{x}_{3\text{ref}} \tag{30}$$

$\dot{x}_3$ is given by (17) and

$$\dot{x}_{3\text{ref}} = A x_1 + B e_2 + C e_3 \tag{31}$$

where A, B and C are defined in the Appendix. Thus, $\dot{V}_3$ is given by

$$\begin{aligned}\dot{V}_3 = &-k_2 e_2^2 \\ &+ \Bigg[u_f + -\left(A + k_1 \frac{EV_L}{X}\cos x_1\right) x_1 \\ &- \left(B - \frac{EV_L}{X}\cos x_1 - a_3\right) e_2 \\ &- C e_3 + \theta\Bigg] e_3 \\ &- \gamma(\theta - \widehat{\theta})\dot{\widehat{\theta}}.\end{aligned} \tag{32}$$

If the adaptation law is chosen as

$$\dot{\widehat{\theta}} = \frac{1}{\gamma} e_3 \tag{33}$$

and the control input is selected as

$$\begin{aligned}u_f = &\left(A + k_1 \frac{EV_L}{X}\cos x_1\right) x_1 \\ &+ \left(B - \frac{EV_L}{X}\cos x_1 - a_3\right) e_2 \\ &+ (C - k_3) e_3 - \widehat{\theta} \quad k_3 > 0\end{aligned} \tag{34}$$

then $\dot{V}_3$ is given by

$$\dot{V}_3 = -k_1 x_1^2 - k_2 e_2^2 - k_3 e_3^2. \tag{35}$$

Since $\dot{V}_3$ is negative definite, global stability of the system (15)–(17) is confirmed. This globally asymptotically stability means that system is stable during large-signal transients regardless of the operating point.

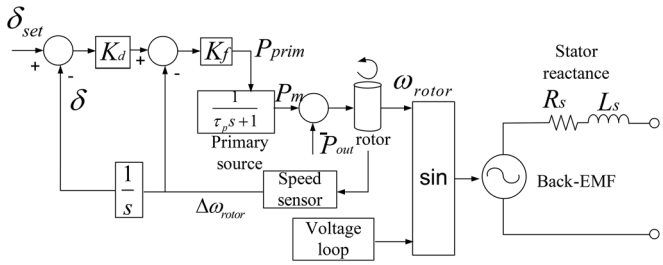

Fig. 5. SG control with angle-frequency control.

V. Discussion About Practicability of the Proposed Controller

As As shown in Fig. 4, the proposed controller has two main parts which are 1) a linear cooperative angle-frequency droop control, and 2) a supplementary nonlinear controller aiming at stabilizing the load angle dynamics during large-angle transients. The only inputs to the linear controller are real and reactive powers which are directly available at the output of the converter. Another advantage of the controller is that the frequency and angle signals are internally available. Moreover, the controller has internal power synchronization and damping dynamics [as defined in (8) and (9)], which provide inherent synchronizing during steady-state and automatically tracks grid frequency and angle deviations, similar to a synchronous machine. This shows that the linear controller can be easily implemented and a supplementary nonlinear signal is generated using (34). To calculate the supplementary control input of the nonlinear controller, according to (34), the perturbations of signals of load angle, frequency and output power $(\Delta\delta, \Delta\omega, \Delta P)$ are required. Toward this, a wash-out filter is employed which adopts angle, frequency and power as input and detects their perturbation. The VSC frequency is available internally and output power can be easily calculated using the measured output current and voltage of the VSC. Using the calculated state variables $\Delta\delta, \Delta\omega, \Delta P$, the control law can be easily implemented in a commercial-grade digital-signal processor (DSP). In other words, all the required variables and control laws can be directly calculated using local information without a need for complex operations or communication. Other practical aspects, such as the presence of conventional SGs in the MG system and noise sensitivity are addressed in the following subsections.

A. Application of Cooperative Angle-Frequency Droop to SGs

As mentioned earlier, one of major advantages of the proposed controller is mimicking the behavior of SGs. Accordingly, the proposed angle-frequency droop can be extended to SGs to ensure nominal steady-state frequency operation whereas power sharing is also achieved. The regular approach for power sharing among SGs is frequency versus real power and voltage versus reactive power droop. In the regular frequency droop of SGs, as the output power of SG is increased, a permanent offset in frequency occurs. Apparently, the droop control is an external control function and is not part of SG behavior. The static equation of SG is given by

$$P_{\text{prim}} = P^*_{\text{SG}} - K_f \omega_{\text{rotor}} \tag{36}$$

where P^*_{SG} is the reference power of the primary source of the SG. Usually, the primary source model is presented by a first-order transfer function [32], [33]. Similar to VSCs, it is possible to deploy the load angle as drooping variable. In this case, the load angle of the SG is directly regulated such that the desirable output power is achieved without permanent frequency offset. In a similar manner, cooperative load angle-frequency is an alternative for power sharing in SGs. In this case, the input power to the SG is governed by

$$P_{\text{prim}} = P^*_{\text{SG}} - K_f \Delta\omega_{\text{rotor}} - K_d K_f \delta. \tag{37}$$

Fig. 5 presents the implementation of cooperative droop control for an SG. The perturbation of the SG rotor speed $\Delta\omega_{\text{rotor}}$ is obtained by processing the measured rotor speed. The load angle is calculated by integration of $\Delta\omega_{\text{rotor}}$. Since the main droop is applied to the load angle, the frequency is maintained constant after the load angle is adjusted. The primary power is applied to the primary source which can be a diesel generator as it generates the reference power with a delay.

B. Effect of Measurements Noise on the Controller

Another issue that the controller may face is the presence of noise in the measured signals. If the proposed cooperative angle-frequency droop control is adopted for VSCs, since only the real and reactive powers are measured through sensors and filtered using a low-pass filter to remove switching effects and obtain the average power, effects of high frequency noises on the powers are automatically eliminated by the low-pass filter. However, if the cooperative angle-frequency droop controller is applied to a real SG, the frequency is not internally available and a speed sensor is necessary to measure the rotor speed. In this case, noise superimposed on the measured speed signal may affect the controller performance because K_f has usually large values; therefore noise effect is intensified and appears in the reference power of the SG. It is worth noticing that K_f is equal to the inverse of m. Since in the conventional frequency droop method, m has small values, K_f usually has large value, thus its effects on the system operation should be investigated. The positive point is the existence of a large rotor with high momentum of inertia which acts as a low-pass filter, and filters out the impact of high frequency noises. In other words, when a white noise with zero average appears in either the input power or measured frequency, its effect is highly attenuated by the rotor dynamics.

VI. Case Studies

To evaluate the validity and effectiveness of the proposed controller, it is applied to two different systems shown in Figs. 6 and 12, which are simulated under the MATLAB/SIMULINK environment. System parameters are given in Tables I and II, respectively. The first system consists of a conventional SG and a VSC-interfaced DG unit. The cooperative droop control without the supplementary nonlinear controller is applied to both units, where power sharing accuracy, constant frequency operation and system transient behavior are investigated. Both units supply a local load and a common load through a transformer and connecting lines. The SIMULINK-based average-

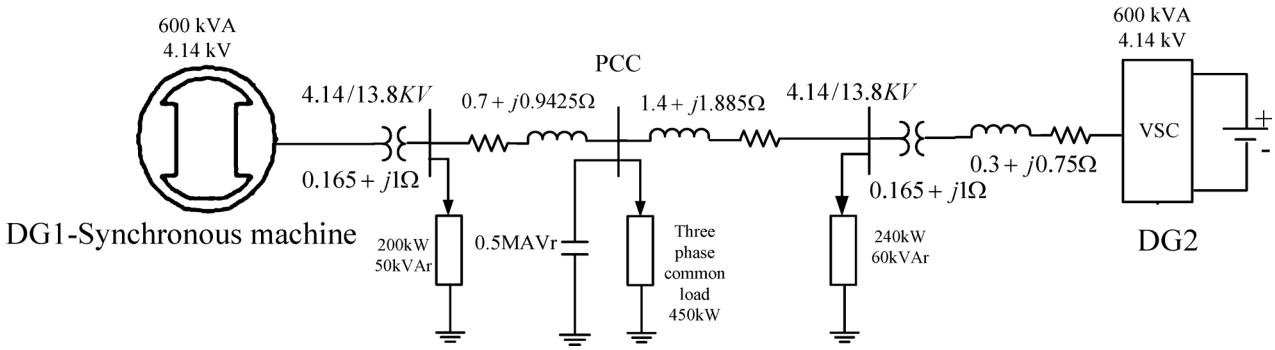

Fig. 6. Configuration of system A.

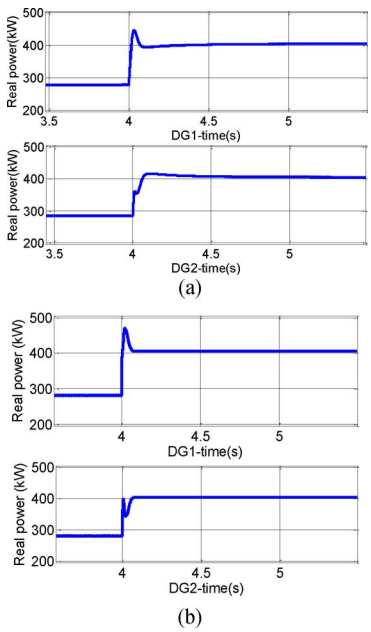

Fig. 7. Real power waveforms of the MG with SG and VSC, (a) with cooperative droop and power loop, and (b) without the angle loop.

model of a VSC and detailed SG model are adopted. The loads consume their rated real and reactive powers at the rated voltage. In this case, the goal is to investigate the practicality of the cooperative droop for SGs and VSCs in various conditions. In the second system (shown in Fig. 12), the MG has three DG units and is connected to a medium-voltage level power system at the PCC through matching transformer. A three-phase matching/isolation transformer is also installed in each DG unit. Each DG has a local load. At the PCC, a sensitive load exists. The MG should supply both sensitive and local loads without interruption. Four scenarios are taken into account; disconnection and reconnection of one unit during islanding, grid restoration and transition to islanding. Static power sharing performance of the MG during islanding is also studied. It should be noted that in all conditions, the controller topology and parameters are not changed.

A. Application of Cooperative Droop to the MG With Conventional SG and VSC

The simulated system in this case is shown in Fig. 6 and it involves two units. The system parameters are given in Table I.

TABLE I
TWO-DG MICROGRID PARAMETERS (ALL PARAMETERS ARE IN SI UNITS)

Parameter	DG1	DG2
Line-line voltage (V)	4140	4140
Stator inductance (L_s)	2mH	-
Stator resistance (R_s)	0.2 Ω	-
K_d	10	10
K_f	1e5	1e5
K_p	-	0.1
Rotor momentum of inertia	10	-
Voltage slope (n)	1e-3	1e-3

TABLE II
THREE-DG MG PARAMETERS (ALL PARAMETERS ARE IN SI UNITS)

Parameter	DG1	DG2	DG3
Line-line voltage (V)	4140	4140	4140
Maximum L-L VSC voltage (V)	4760	4760	4760
K_d	100	120	80
K_f	1e5	1e5	1e5
K_p	0.1	0.1	0.1
Voltage slope (n)	2.5e-4	2e-4	3e-4
ω_c	200	200	200

The cooperative droop is applied to both the SG and VSC to evaluate its practicality for different types of generation units. Two controllers topologies are taken into account to study the effect of frequency restoration; the first controller involves both angle and frequency droops whereas in the second controller, only the frequency loop exists and the angle drooping is removed ($K_d = 0$) (i.e., only frequency droop is enabled). Initially, DG units supply a common 180 kW load. At $t = 4$ s, the common load power is increased to 450 kW and at $t = 5.5$ s, a 100 kW single phase load is connected to the PCC. Figs. 7 and 8 exhibit the power and frequency waveforms before and after the load power variation for both cooperative droop control and frequency droop methods. As it can be seen, power sharing error for both controllers before and subsequent to load power change is less than 0.5%. Nevertheless, in the system in which

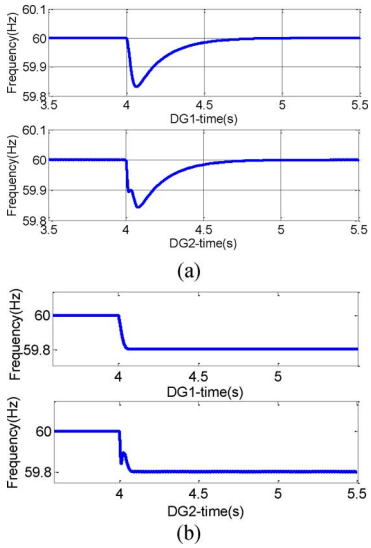

Fig. 8. Frequency waveforms of the MG with SG and VSC, (a) with cooperative droop and power loop, and (b) without the angle loop ($K_d = 0$).

cooperative droop is employed, the rated frequency is recovered in less than 0.5 s whereas in the system with pure frequency drooping control, a permanent frequency offset equal to 0.2 Hz is occurs. This is because when $K_d = 0$, system characteristics equation converges to (36), which yields a permanent frequency drop. From the power quality perspective, it is important to have constant frequency operation because most of modern loads are sensitive to frequency deviations and it may adversely affect their operation. Whenever frequency droop in an MG is employed, proper operation of sensitive loads, when steady state frequency varies in a wide range, is a major concern. In this case, the system without the angle droop loop still presents satisfactory dynamic performance similar to the cooperative angle frequency controller which is due to existence of the extra power loop. Further, the maximum overshoot in the SG's real power is reduced from 475 kW to 445 kW with the hybrid droop control due to the improved dynamic performance.

1) Effect of Speed Sensor Noise on Controller Performance: The controller performance with and without the presence of white noise in the SG's speed sensor are compared. Toward this, a white noise with average amplitude between 0.2–0.3 Hz is added to the measured speed as shown in Fig. 9(a). The actual rotor speed and output power waveforms are shown in Fig. 9(b) and (c), respectively. It is obvious that noise doesn't have a considerable effect on the output power and actual rotor speed as the rotor inertia filters out high-frequency disturbances.

2) Unbalanced System: In this scenario, it is supposed that the system initially supplies the common 450 kW load and at $t = 5.5$ s, a 25 kW single phase load is connected to the phase b at PCC. The power waveforms after this event are shown in Fig. 10. The single phase load causes power oscillations with amplitude of 7 kW with the average power equal to 416 kW. The real power is still shared equally between DG units. The ratio of negative and positive components of voltage is less than 2.6% which is within the acceptable typical unbalance limits. System stability is also preserved during unbalanced condition. It should be noted that in this scenario, the positive sequence of

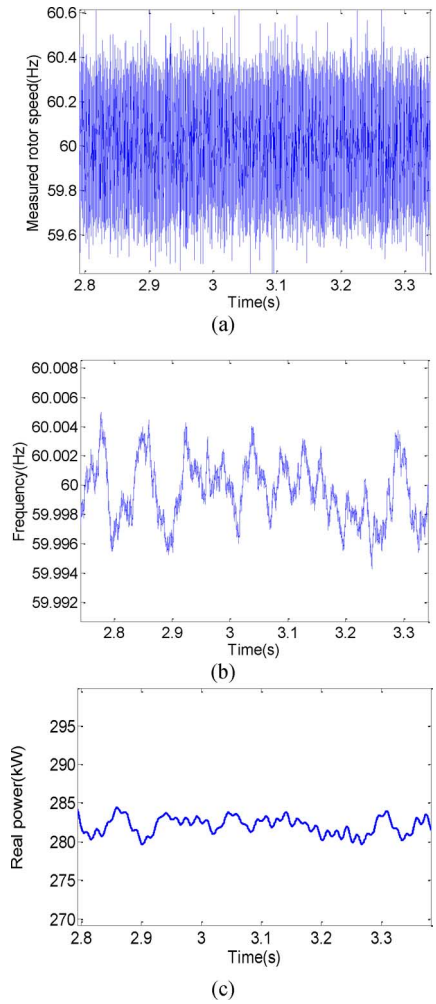

Fig. 9. Effect of noise on the system performance, (a) measured rotor frequency, (b) actual rotor frequency, and (c) output power.

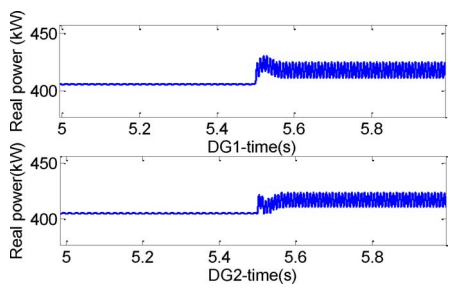

Fig. 10. Effect of switching of a single phase load at PCC.

the real and reactive powers are used for control purposes rather than the total real and reactive powers. It should be noted that unbalanced condition is out of scope of this paper. Although the controller presents satisfactory performance, to get better power sharing accuracy and lower negative-sequence voltage, virtual impedance shaping can be integrated into the negative voltage control loop [34] or online set-point adjustment [35] can be employed which can be addressed in future work.

3) Effect of SG's Primary Mover: In the previous studies, for the sake of simplicity, the dynamics of the primary source was ignored, i.e., $\tau_p = 0$. However, as shown in Fig. 5, in reality,

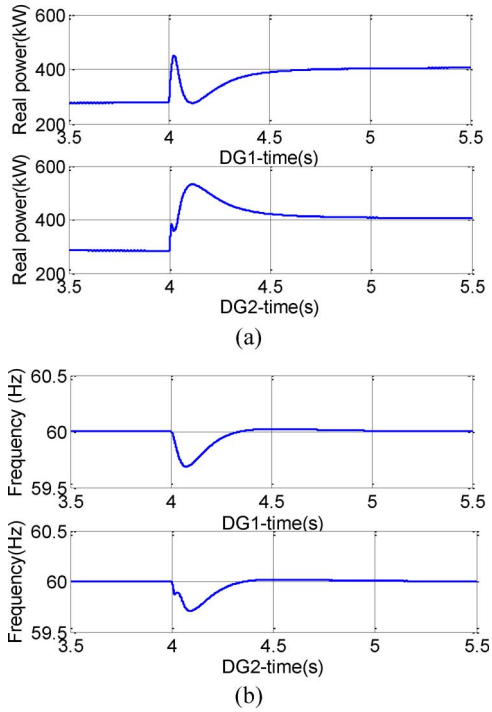

Fig. 11. Effect of the SG's primary source with $\tau_p = 0.5$ s on system performance, (a) real power and (b) frequency.

the SGs are supplied by a primary mover that generates its reference power with some delay. In this case, the dynamics of the primary source is taken into account, and it is supposed the SG is fed by a slow diesel engine with time constant (τ_p) equal to 0.5 s to study the effect of the primary source on power sharing and system dynamics. Other parameters are similar to those given in Table I. The simulation results with consideration of primary mover dynamics before and after load power change are given in Fig. 11. Fig. 11 reveals that accurate power sharing with error less than 0.5% is achieved at nominal steady-state frequency operation. The frequency recovery time is about 1.0 s. It is also noticeable that the dynamic performance is degraded as compared to the previous case. Also during the transient period, since VSC's source is considered as an ideal one without delay, the VSC mainly provides MG's power causing more overshoot in its output power. In other words, the degraded dynamic performance is mainly caused by different time constants and dynamic behaviors of primary sources of VSC and SG. Simply speaking, the higher the time constant of the SG's primary source, the worse dynamic performance and more interaction between units is yielded.

B. MG With Three DG Units and Supplementary Control

1) Case 1: Disconnection of DG2: The model shown in Fig. 12 is simulated to evaluate the performance of the control system with nonlinear cooperative droop control. The controller parameters are given in Table II. It is supposed that the MG initially works in islanding mode, and then it is reconnected to the grid. The sequence of events is as follows: at $t = 0.8$ s, DG2 is disconnected and DG1 and DG3 supply the total MG load demand. At $t = 1.5$ s, DG1 is again connected to the MG. At $t = 2.5$ s, the static switch is closed and the grid is restored. At $t = 3$ s, again an islanding event occurs. All these scenarios are considered as large-signal disturbances, where DGs output powers, frequencies and load angles rapidly change in a wide range. It is assumed that the MG initially works in islanding mode and all DGs and loads are connected. At $t = 0.8$ s, DG2 is disconnected from the MG and DG1 and DG3 supply local load of DG2. The power waveforms with the supplementary control are shown in Fig. 13. Before DG2 disconnection, the generated power of DG1, DG2 and DG3 are 2.06, 2.43 and 1.645 MW, respectively, which are very close to their desirable ratio (4:5:6) and the maximum error in power sharing is less than 1.5%. It should be noted the main assumption here is that DG units have enough power capacity to supply the total MG load demand. As it can be seen from Fig. 13, after DG2 disconnection, the output power of DG1 and DG3 still remain within their power capacities. If this is not the case and DG units cannot provide the load power demand, a load shedding strategy, as presented in [36], should be applied to shed non-critical loads. However, this paper just deals with stability issues of MG under generation-load matching conditions, which is a necessary but not sufficient condition for overall MG stability. After the DG outage, the system with the supplementary control exhibits fully damped behavior without any overshoot.

2) Case 2: Reconnection of DG2 With Out-of-Phase Reclosing: In this section, the transient behavior of the MG after reconnection of DG1 is investigated. Again, this scenario is considered as a large-signal disturbance because DG2 which forms 40% of the total MG power capacity is reconnected without any synchronization process. Note that any considerable difference between voltage angle of DG2 and the MG at the point of connection is considered as large disturbance and results in severe transients. The power waveforms with and without the supplementary nonlinear controller are shown in Fig. 14. The effectiveness of the nonlinear controller in this case is obviously pronounced and the system with the supplementary nonlinear controller offers much better transient performance compared to the linear system. Actually, the nonlinear controller adjusts VSC voltage such that it damps angle, frequency and power fluctuations.

3) Case 3: Grid Restoration With Out-of-Phase Reclosing: In the grid connected mode, DG units are required to inject their reference powers and there is no need to share power. Thus, the output powers of DG units are abruptly changed subsequent to connection to the grid to their reference values. During grid connection, DG1, DG2 and DG3 generate 2.38 MW, 2.86 MW and 1.9 MW, respectively. In this scenario, the static switch at the PCC is suddenly closed and the utility grid is restored. The power waveforms are illustrated in Fig. 15. Note that no synchronization process is applied and connection is abrupt without any information from the grid voltage. In fact, to connect the MG to the main grid seamlessly, the angle and voltage mismatch between two sides of the static switch should be near to zero. Any considerable error between phase, frequency and amplitude of the MG and the utility grid voltages at PCC may cause severe oscillations, high currents and even instability. High current may flow to the circuit subsequent to grid connection. This scenario is similar to the out-of-phase reclosing event that might take place when a DG unit (or a micro-grid) is not

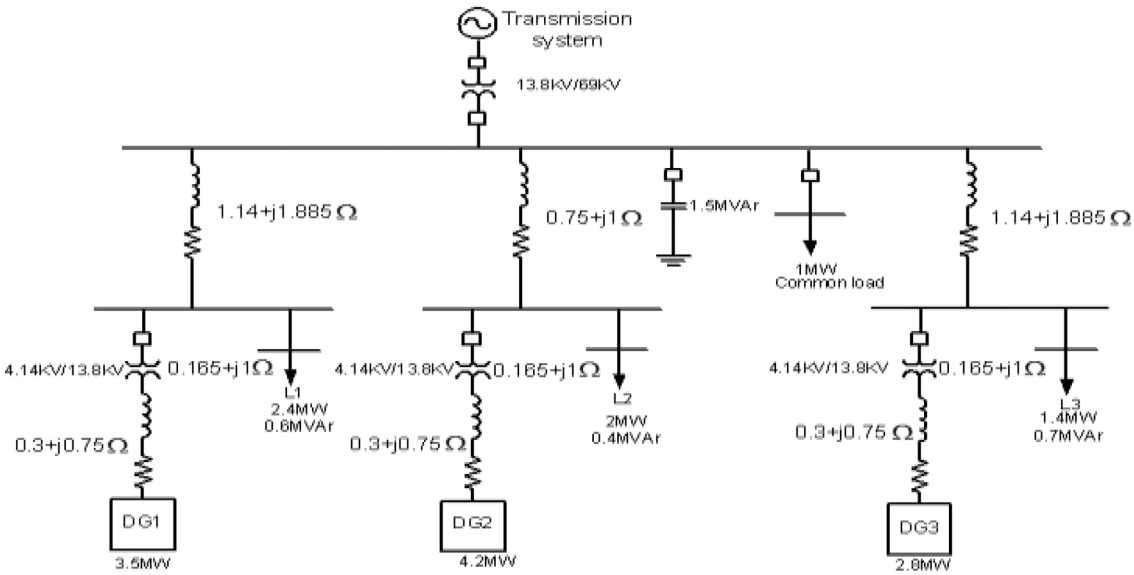

Fig. 12. Configuration of system B.

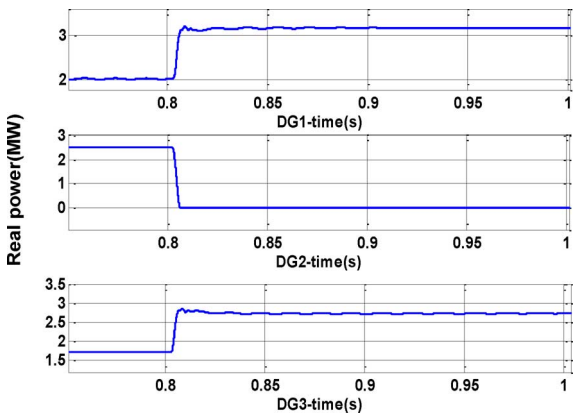

Fig. 13. Power waveforms of case *B1*.

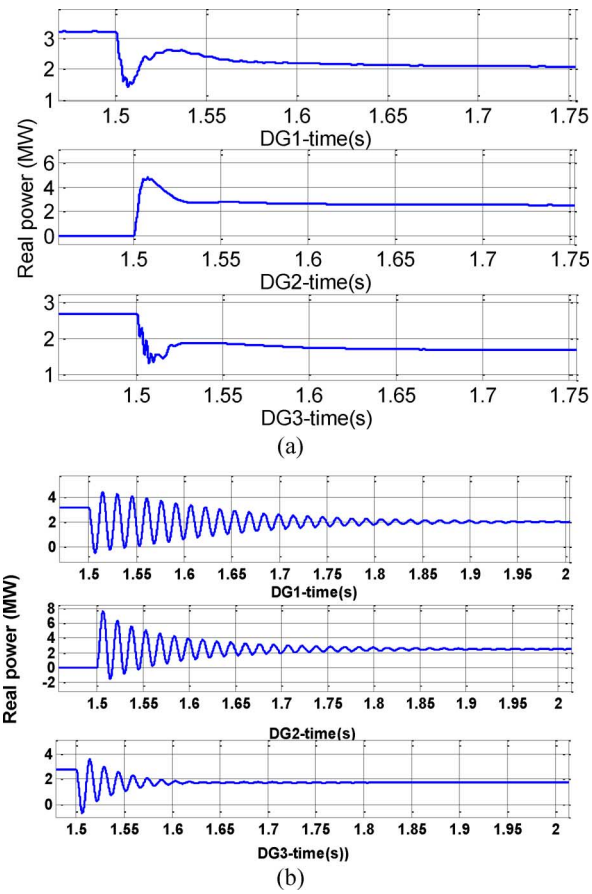

Fig. 14. Power waveforms of case B2, (a) with, and (b) without the supplementary controller.

disconnected upon a temporary fault in a feeder equipped with auto-recloser. Nevertheless, by proper adjustment of voltages of the DG units during grid connection using the supplementary controller, power, frequency, angle and current are kept within the acceptable limits. Fig. 16 shows the current waveforms of DG3, as a sample, during grid connection, which clearly confirms that no considerable current overshoot occurred; only for one cycle some minor overshoot in the phase current is observed. On the contrary, any instability in the load angle and frequency may result in high current flowing to the circuit. In fact, the duty of the nonlinear controller is to adjust the voltage amplitude such that the load angle and frequency stability is preserved, which automatically results in smooth current waveforms during grid connection. In other words, the "plug and play" concept is achieved via the proposed nonlinear cooperative control. Otherwise, grid connection without verifying the synchronization process and without using the nonlinear controller may cause severe overshoot in power and current. The same problem also exists in Case 2, where voltage angle and amplitude mismatch between DG2 and the MG at the point of their connection generates severe transients. Similar to case 2, nonlinear-controlled DGs have smooth and well damped performance during grid connection while the linear controller-based MG exhibits poor transient behavior. Again, in this case, the nonlinear controller adjusts the DG voltage reference such that angle, frequency and power

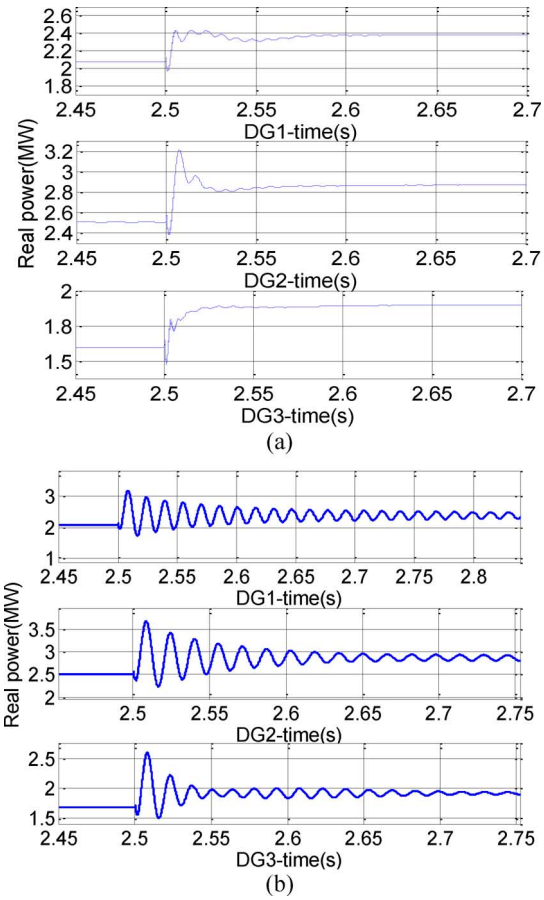

Fig. 15. Power waveforms of case B3, (a) with, and (b) without the supplementary controller.

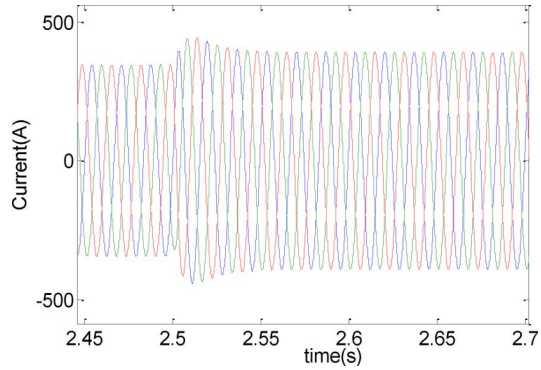

Fig. 16. Current waveforms of DG3 during grid connection using supplementary nonlinear controller.

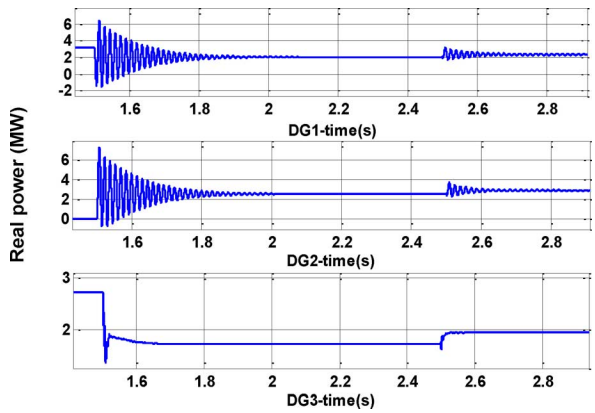

Fig. 17. Power waveforms of case B4. DG1 and DG2 without nonlinear controller and DG3 with the supplementary nonlinear controller.

fluctuations are minimized. It should be noted that frequency and angle oscillations depend on damping and synchronizing powers, respectively. The damping and synchronizing powers are proportional to K_f and K_d, respectively, according to (8) and (9). By increasing these constants, more damped power and frequency with faster convergence can be obtained at the cost of poor static performance and power sharing. However, the nonlinear supplementary controller provides the necessary damping under wide range of operating conditions and droop parameters without loss of stability. The synchronization problems and out-of-phase reclosing are the best scenarios to test nonlinear controllers because any large difference in angle and frequency between two sides of switch at the moment of connection is a large-signal disturbance and leads to severe transients.

4) Case 4: DG2 Reconnection and Grid Restoration—DG1 and DG2 Without and DG3 With Nonlinear Controller: In this section, the ability of the nonlinear controller to overcome interactions between DG units is investigated. Toward this, a scenario is taken into account in which DG 1 and DG2 use the linear angle-frequency droop whereas DG3 uses the nonlinear supplementary controller. Similar to case 2 and 3, at $t = 1.5$ s, DG2 is connected to the MG and at $t = 2.5$ s, the static switch is closed. It is evident from Fig. 17 that at the moment of reconnection of DG2, its output power starts to oscillate and due to its interaction with DG1, power of DG1 also fluctuates. That is to say that instability and oscillations propagate within the MG. On the contrary, DG3 has smooth operation in both scenarios. This case shows the ability of the nonlinear supplementary control to mitigate instabilities due to interaction between DG units which is one of its remarkable features.

5) Case 5: Islanding: Another scenario that frequently occurs in an MG system is transition from grid connection to islanding mode. When a fault occurs in the grid, it is necessary to disconnect the MG from the main grid. The proposed angle-frequency droop control has the ability to work in both modes without change in the controller structure. Consequently, the problems due to islanding detection are inherently eliminated. The power sharing is automatically achieved by droop constants K_f and K_d, whereas these constants are employed as damper and synchronizer during grid connection. The power waveforms of DG units subsequent to islanding are presented in Fig. 18. In this case, the transition to islanding is seamless with minimum fluctuation, which proves the effectiveness of the combined droop controller. In the cases such as synchronization issues, in which any large angle and frequency error between two sides of connection results in large signal disturbance the supplementary nonlinear controller can significantly enhance system stability and realize the concept of DG plug and play. Frequency waveforms of different DG units between $t = 0.75$ s and 3.0 s in the system with the nonlinear controller are shown

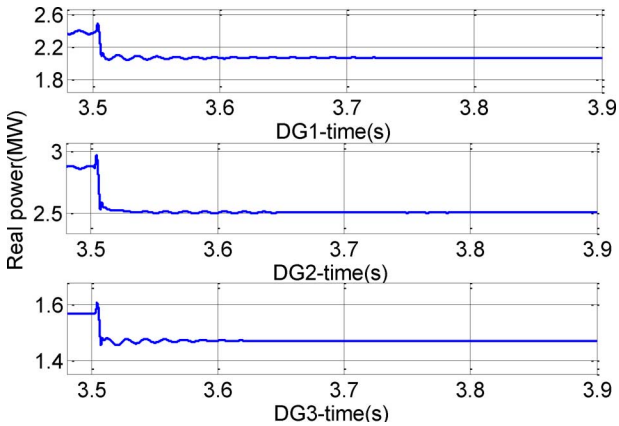

Fig. 18. Power waveforms subsequent to islanding.

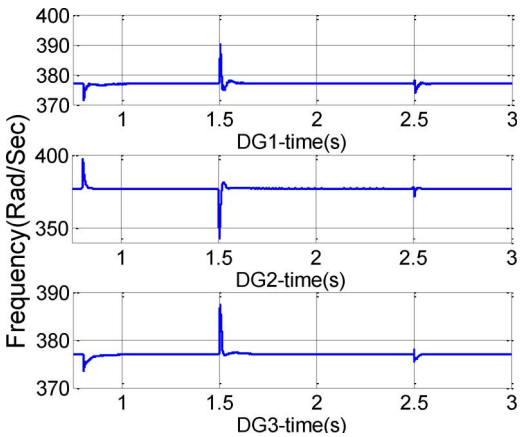

Fig. 19. Frequency variations in MG with the supplementary control.

in Fig. 19, which shows fixed nominal-frequency steady-state operation of the MG in both modes, which is one of benefits of the proposed hybrid controller.

VII. Conclusion

A comprehensive and general power management/control strategy for both converter- and synchronous machines-based DG units in islanded and grid-connected MGs has been developed in this paper. The proposed combined angle-frequency droop control can fulfill accurate power sharing, constant nominal-frequency operation at steady-state and stable performance in a wide range of operating conditions. However, in large sudden contingencies such as connection and disconnection of DG units and out-of-phase closing, using a linear controller cannot ensure stable MG operation. To overcome this problem and guarantee large-signal stability of the MG, a nonlinear supplementary controller has been developed for the linear droop control. The adaptive backstepping technique has been employed to design the nonlinear controller and overcome modeling uncertainties. The effectiveness of the proposed controller is evaluated by simulation results under typical MG operating conditions.

Appendix

Definition of constants A, B and C:

$$A = K_f - k_1^2 K_f + k_1 K_d K_f - 2k_1 K_p + \frac{k_1^3}{K_p} - \frac{k_2}{K_p}$$

$$B = (k_1 + k_2 - K_d)K_f + \frac{1 - k_1^2 - k_2^2 - k_1 k_2}{K_p}$$

$$C = -k_1 - k_2 + K_p K_f.$$

References

[1] A. Guerrero *et al.*, "Distributed generation," *IEEE Ind. Elect. Mag.*, pp. 52–64, Mar. 2010.

[2] N. Hatziargyriou, H. Asano, R. Iravani, and C. Marnay, "Microgrids," *IEEE Power Energy Mag.*, vol. 5, no. 4, pp. 78–94, Jul./Aug. 2007.

[3] F. Katiraei and M. R. Iravani, "Power management strategies for a microgrid with multiple distributed generation units," *IEEE Trans. Power Syst.*, vol. 21, no. 4, pp. 1821–1831, Nov. 2006.

[4] *IEEE Standard for Interconnecting Distributed Resources With Electric Power Systems*, IEEE Std. 1547-2003.

[5] *IEEE Guide for Monitoring, Information Exchange, and Control of Distributed Resources Interconnected With Electric Power Systems*, IEEE 1547.3-2007, 2007.

[6] J. C. Vasquez, R. A. Mastromauro, J. M. Guerrero, and M. Liserre, "Voltage support provided by a droop-controlled multifunctional inverter," *IEEE Trans. Ind. Elect.*, vol. 56, no. 11, pp. 4510–4519, Nov. 2009.

[7] E. Santacana, G. Rackliffe, L. Tang, and X. Feng, "Getting smart," *IEEE Power Energy Mag.*, vol. 8, no. 2, pp. 41–48, Mar./Apr. 2010.

[8] C. Yuen, A. Oudalov, and A. Timbus, "The provision of frequency control reserves from multiple microgrids," *IEEE Trans. Ind. Elect.*, vol. 58, no. 1, pp. 173–183, Jan. 2011.

[9] X. Yuan and Y. Zhang, "Status and opportunities of photovoltaic inverters in grid-tied and micro-grid systems," in *Proc. IEEE 5th Int. Power Electronics and Motion Control Conf., IPEMC 2006*.

[10] Y. A.-R. I. Mohamed and E. F. El-Saadany, "Adaptive decentralized droop controller to preserve power sharing stability of paralleled inverters in distributed generation microgrids," *IEEE Trans. Power Elect.*, vol. 23, no. 26, pp. 2806–2816, Nov. 2008.

[11] J. M. Guerrero, L. Hang, and J. Oceda, "Control of distributed uninterruptable power supplies," *IEEE Trans. Ind. Elect.*, vol. 50, no. 8, pp. 2845–2859, Aug. 2008.

[12] A. G. Tsikalakis and N. D. Hatziagrion, "Centralized control for optimizing microgrid operation," *IEEE Trans. Energy Convers.*, vol. 23, no. 1, pp. 241–248, Mar. 2008.

[13] R. Majumder, "Power sharing and control in distributed generation with wireless sensor network," *IEEE Trans. Smart Grid*, vol. 3, no. 2, pp. 618–634, Jun. 2012.

[14] I. Chung *et al.*, "Control methods of inverter-interfaced distributed generators in a microgrid system," *IEEE Trans. Ind. Appl.*, pp. 1078–1088, May/Jun. 2010.

[15] J.-F. Chen and C.-L. Chu, "Combination voltage controlled and current controlled PWM inverters for UPS parallel operation," *IEEE Trans. Power Elect.*, vol. 10, no. 5, pp. 547–558, Sep. 1995.

[16] S. Ahn *et al.*, "Power-sharing method of multiple distributed generators considering modes and configurations of a microgrid," *IEEE Trans. Power Del.*, vol. 25, no. 3, pp. 2007–2016, Jul. 2010.

[17] K. D. Brabandes *et al.*, "A voltage and frequency droop control method for parallel inverters," *IEEE Trans. Power Elect.*, vol. 22, no. 4, pp. 1107–1114, Jul. 2007.

[18] J. Guerrero, J. C. Vasquez, and L. G. D. Vicuna, "Hierarchical control of droop-controlled AC and DC microgrids-A general approach toward standardization," *IEEE Trans. Ind. Elect.*, vol. 58, no. 1, pp. 158–166, Jan. 2011.

[19] E. Baklund *et al.*, "Energy management in autonomous microgrids using stability-consternated droop control of inverter," *IEEE Trans. Power Elect.*, vol. 23, no. 5, pp. 2346–2351, Sep. 2008.

[20] R. Majumder *et al.*, "Improvement of stability and load sharing in an autonomous microgrid using supplementary droop control loop," *IEEE Trans. Power Syst.*, vol. 25, no. 2, pp. 796–808, May 2010.

[21] J. Kim *et al.*, "Mode adaptive droop control with virtual output impedances for an inverter-based flexible microgrid," *IEEE Trans. Power Elect.*, vol. 26, no. 3, pp. 698–701, Mar. 2011.
[22] R. Majumder *et al.*, "Droop control of converter-interfaced microsources in rural distributed generation," *IEEE Trans. Power Del.*, vol. 25, no. 4, pp. 2768–2778, Oct. 2010.
[23] R. Majumder, A. Ghosh, G. Ledwich, and F. Zare, "Angle droop versus frequency droop in a voltage source converter based autonomous microgrid," in *Proc. IEEE Power & Energy Society General Meeting*, 2009.
[24] Q. Zhong and G. Weiss, "Synchronverters: Inverters that mimic synchronous generators," *IEEE Trans. Ind. Elect.*, vol. 58, no. 4, pp. 1259–1267, Apr. 2011.
[25] M. F. M. Arani and E. F. El-Saadani, "Implementing virtual inertia in DFIG-based wind power generation," *IEEE Trans. Power Syst.*, to be published.
[26] M. Zhixin, F. Lingling, D. Osborn, and S. Yuvarajan, "Wind farms with HVDC delivery in inertial response and primary frequency control," *IEEE Trans. Energy Convers.*, vol. 25, no. 4, pp. 1171–1178, Dec. 2010.
[27] J. Zhu, C. D. Booth, G. P. Adam, A. J. Roscoe, and C. G. Bright, "Inertia emulation control strategy for VSC-HVDC transmission systems," *IEEE Trans. Power Syst.*, to be published.
[28] T. L. Vandoorn *et al.*, "Directly-coupled synchronous generators with converter behavior in islanded microgrids," *IEEE Trans. Power Syst.*, vol. 27, no. 3, pp. 1395–1406, Aug. 2012.
[29] P. Kundur, *Power System Stability and Control*. New York, NY, USA: McGraw-Hill, 1994.
[30] A. Karimi and A. Feliachi, "Decentralized adaptive backstepping of electric power systems," *Elect. Power Syst. Res.*, vol. 78, no. 3, pp. 484–493, 2008.
[31] R. Yan, Z. Y. Dong, T. K. Saha, and R. Majumder, "A power system nonlinear adaptive decentralized controller design," *Automatica*, vol. 46, no. 2, pp. 330–336, 2010.
[32] P. H. Divshali, A. Alimardani, S. H. Hosseinian, and M. Abedi, "Decentralized cooperative control strategy of microsources for stabilizing autonomous VSC-based microgrids," *IEEE Trans. Power Syst.*, vol. 27, no. 4, pp. 1949–1959, Nov. 2012.
[33] Dynamics and Control of Electric Power Systems, Lecture, EEH—Power Systems Laboratory, ETH. Zürich, Switzerland.
[34] M. Hamzeh, H. Karimi, and H. Mokhtari, "A new control strategy for a multi-bus MV microgrid under unbalanced conditions," *IEEE Trans. Power Syst.*, vol. 27, no. 4, pp. 2225–2232, Nov. 2012.
[35] A. Mehrizi-Sani and R. Iravani, "Online set point adjustment for trajectory shaping in microgrid applications," *IEEE Trans. Power Syst.*, vol. 27, no. 1, pp. 216–223, Feb. 2012.
[36] I. J. Balaguer *et al.*, "Control for grid-connected and intentional islanding operation of distributed power generation," *IEEE Trans. Ind. Elect.*, vol. 58, no. 1, pp. 147–156, Jan. 2011.

Seyed Mahdi Ashabani was born in Isfahan, Iran. He received the B.Sc. degree in electrical engineering from Isfahan University of Technology, Isfahan, Iran, and the M.Sc. degree from Amirkabir University of Technology (Tehran Polytechnic), Tehran, Iran, both with honors. He is now pursuing the Ph.D. degree at the University of Alberta, Edmonton, AB, Canada.

His research interests cover many aspects of power engineering including smart grids, microgrids, power electronics and design and optimization of magnetic devices.

Yasser Abdel-Rady I. Mohamed (M'06–SM'011) was born in Cairo, Egypt, on November 25, 1977. He received the B.Sc. (with honors) and M.Sc. degrees in electrical engineering from Ain Shams University, Cairo, Egypt, in 2000 and 2004, respectively, and the Ph.D. degree in electrical engineering from the University of Waterloo, Waterloo, ON, Canada, in 2008.

He is currently with the Department of Electrical and Computer Engineering, University of Alberta, Edmonton, AB, Canada, as an Associate Professor. His research interests include dynamics and controls of power converters; distributed and renewable generation; modeling, analysis and control of smart grids; electric machines and motor drives.

Dr. Mohamed is an Associate Editor of the IEEE TRANSACTIONS ON INDUSTRIAL ELECTRONICS. He is also a Guest Editor of the IEEE TRANSACTIONS ON INDUSTRIAL ELECTRONICS Special Section on "Distributed Generation and Microgrids". His biography is listed in Marque's Who is Who in the World. He is a registered Professional Engineer in the Province of Alberta.